fibers

MDPI

Article

Finite Element Modelling of Pultruded FRP Beam-to-Column Joints

Jawed Qureshi * and Karthick Murugan Mahendran

School of Architecture, Computing and Engineering (ACE), University of East London, 4-6 University Way, Beckton, London E16 2RD, UK
* Correspondence: j.qureshi@uel.ac.uk; Tel.: +44-020-8223-2363

Highlights

What are the main findings?

- A finite element model combining Hashin's failure criterion and fracture energy-based damage evolution accurately predicted FRP joint behaviour, matching experiments within 10%.
- Delamination at the fillet radius governed failure, while cleat thickness and bolt size increased stiffness by up to 15% without reducing strength.

What is the implication of the main finding?

- The validated FEM provides a cost-effective tool for designing and optimising pultruded FRP beam-to-column joints.
- The study supports reliable design guidelines for FRP structures, classifying the joints as nominally pinned as per Eurocodes.

Abstract

This research addresses the critical gap in accurately modelling pultruded fibre-reinforced polymer (FRP) beam-to-column joints, where previous studies largely ignored progressive damage mechanisms. A novel finite element framework is developed in ABAQUS, integrating Hashin's failure criterion with fracture energy-based damage evolution to simulate delamination and brittle failure in FRP cleats. The model is rigorously validated against full-scale experimental data, achieving close agreement in moment–rotation response, initial stiffness (within 5%), and ultimate moment capacity (variation < 10%). Quantitative results confirm that delamination at the fillet radius governs failure, while qualitative analysis reveals the sensitivity of stiffness to cleat geometry and bolt characteristics. A parametric study demonstrates that increasing cleat thickness and bolt diameter enhances stiffness up to 15%, whereas bolt–hole clearance introduces slip without significantly affecting strength. The validated FEM reduces reliance on costly physical testing and provides a robust tool for optimising FRP joint design, supporting the future development of design guidelines for pultruded FRP structures.

Keywords: FRP connections; finite element analysis; bolted joints; Hashin's damage criterion; delamination; fracture mechanics

check for updates

Academic Editor: Martin J. D. Clift

Received: 22 September 2025
Revised: 22 October 2025
Accepted: 30 October 2025
Published: 7 November 2025

Citation: Qureshi, J.; Mahendran, K.M. Finite Element Modelling of Pultruded FRP Beam-to-Column Joints. *Fibers* **2025**, *13*, 151. https://doi.org/10.3390/fib13110151

Copyright: © 2025 by the authors. Licensee MDPI, Basel, Switzerland. This article is an open access article distributed under the terms and conditions of the Creative Commons Attribution (CC BY) license (https://creativecommons.org/licenses/by/4.0/).

1. Introduction

Fibre-reinforced polymer (FRP) materials are increasingly used in structural engineering due to their high strength-to-weight ratio, corrosion resistance, and durability [1,2]. Pultruded FRP profiles, manufactured through a continuous process, offer consistent

mechanical properties, making them suitable for structural applications such as bridges, buildings, and offshore platforms [3]. Despite these advantages, the adoption of FRP structures remains limited due to a lack of established design guidelines and uncertainty regarding their long-term performance [4].

A critical challenge in FRP structures is the design of bolted beam-to-column connections, which significantly influence overall frame stability and load transfer [5]. Unlike steel joints, FRP joints exhibit different failure mechanisms, including delamination and fibre–matrix debonding, which affect their moment–rotation behaviour [6]. Experimental studies have provided valuable insights into the performance of FRP connections [7–9]. However, physical testing is time-consuming and costly. Finite element modelling (FEM) offers an efficient alternative to predict joint behaviour and reduce experimental dependencies [3]. A detailed review of fibre-reinforced polymer joints is presented in the first author's well-known paper [10].

Several researchers have investigated the behaviour of pultruded fibre-reinforced polymer (FRP) beam-to-column connections using finite element modelling (FEM) approaches. The main focus of these studies has been on modelling linear–elastic anisotropic behaviour of FRP materials without considering progressive damage. Eskenati et al. [11] examined adhesively bonded and bolted connections in pultruded glass FRP profiles by assuming linear–elastic behaviour and transverse isotropy within ABAQUS. Progressive damage was not considered. The GFRP profiles were connected 120°or 160° to represent arched structures for tunnelling applications. The joints' arrangement was not typical beam-to-column joints.

The pin-bearing strength of FRP plate-to-plate connections has been investigated experimentally [12] and numerically by Coelho and Mottram [13]. The FRP plates were modelled as stacked continuum shell elements. In this approach, the FRP plate was represented as a laminate comprising 11–14 stacked layers with varying properties. These layers consisted of continuous filament mat and unidirectional glass fibre rovings, with adhesive elements introduced between successive layers. Distinct material properties were defined for each layer. This modelling technique provides a sufficiently accurate representation for small-scale models; however, its application to structural FRP frames and beam–column joint sub-assemblies would be challenging due to the associated computational demands. The cyclic behaviour of steel-reinforced concrete beam–column joints has been investigated both experimentally and numerically in the research by Duan et al. [14]. Similarly, for pultruded FRP beam-to-column joints, cyclic behaviour has been examined experimentally by Qureshi et al. [15].

Recent studies have highlighted the challenges associated with achieving efficient and reliable connections in pultruded FRP frames. Tang et al. [16] conducted a comprehensive state-of-the-art review of beam–column joints, noting that most joints exhibit pinned or semi-rigid behaviour with limited strength utilisation, and that current design guidelines lack sufficient provisions for joint design. This demonstrates the need for improved modelling and design methods. Complementing this, Ascione et al. [17] proposed a novel ductile hybrid connection combining bonded FRP members with bolted steel elements designed to be weaker than the FRP profiles. Their experimental work demonstrated that this approach provides adequate stiffness, resistance, and significantly enhanced ductility, while ensuring repairability through replaceable steel components. Together, these studies underline the importance of developing reliable numerical models and innovative joint solutions—objectives that are directly addressed in the present research.

Despite advancements, limited research exists on finite element analysis of FRP joints using progressive collapse methods [4,18]. Most previous studies focused on experimental investigations, leaving a gap in numerical modelling approaches. Considering the highly

anisotropic nature and the linear–elastic, brittle behaviour of FRP materials, there has been limited success in effectively modelling FRP shapes and systems. Developing reasonably accurate FEM models is essential to predict stiffness, moment resistance, and failure modes in FRP joints. The application of Hashin's damage criterion and progressive damage modelling can improve the accuracy of these simulations.

This study aims to develop and validate an FEM model for bolted beam-to-column FRP joints using ABAQUS. The model is designed to predict moment–rotation behaviour, initial stiffness, and delamination crack initiation. A parametric study investigates the effects of cleat size, bolt size, and hole clearance. The findings will provide a reliable numerical framework for FRP structural design, reducing reliance on costly experimental testing.

2. Finite Element Model—Validation

Full-scale tests on pultruded fibre-reinforced polymer (FRP) beam-to-column joints from Qureshi and Mottram [18] are used to validate the three-dimensional finite element model. The finite element model, including boundary conditions, material properties, loading configuration, and analysis procedure, is described below.

2.1. Description of Experimental Setup

The experimental arrangement [18] shown in Figure 1 is used to validate the finite element (FE) model. The setup features a major-axis beam-to-column joint, where two cantilever beams are connected to a central column using a pair of web cleats. Vertical load is applied at the free ends of the back-to-back beams.

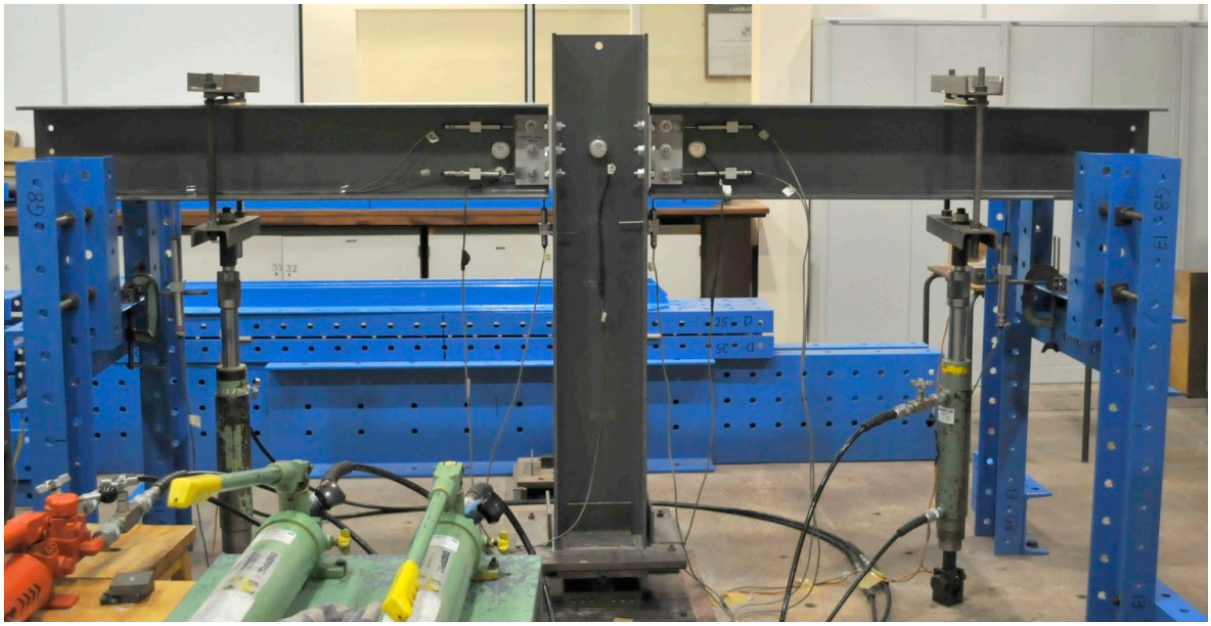


Figure 1. Photograph of back-to-back beam-to-column joint sub-assembly [18].

Both the beams and the column are 1500 mm long and consist of wide flange (WF) sections with dimensions of 254 × 254 × 9.53 mm. The web cleats, 192 mm in height, are cut from an equal angle. The connection incorporates an equal-leg angle web cleat with dimensions of 100 × 100 × 9.53 mm, where the leg lengths are 100 mm each and the thickness is 9.53 mm. The reinforcement in the cleats is aligned with the direction of the applied shear force. The reinforcement in the cleats refers to the unidirectional glass fibres embedded within the pultruded GFRP material, which are aligned parallel to the leg length of the cleats to replicate the actual manufacturing orientation. The beam centreline is

positioned 1094 mm above the base of the column. The column base rests on a steel rocker fixture that permits in-plane rotation, justifying the assumption of a pinned connection. This pinned support ensures equal loading on both beams during testing. All dimensions, general arrangement of the test, and connection detailing are presented in Figure 2.

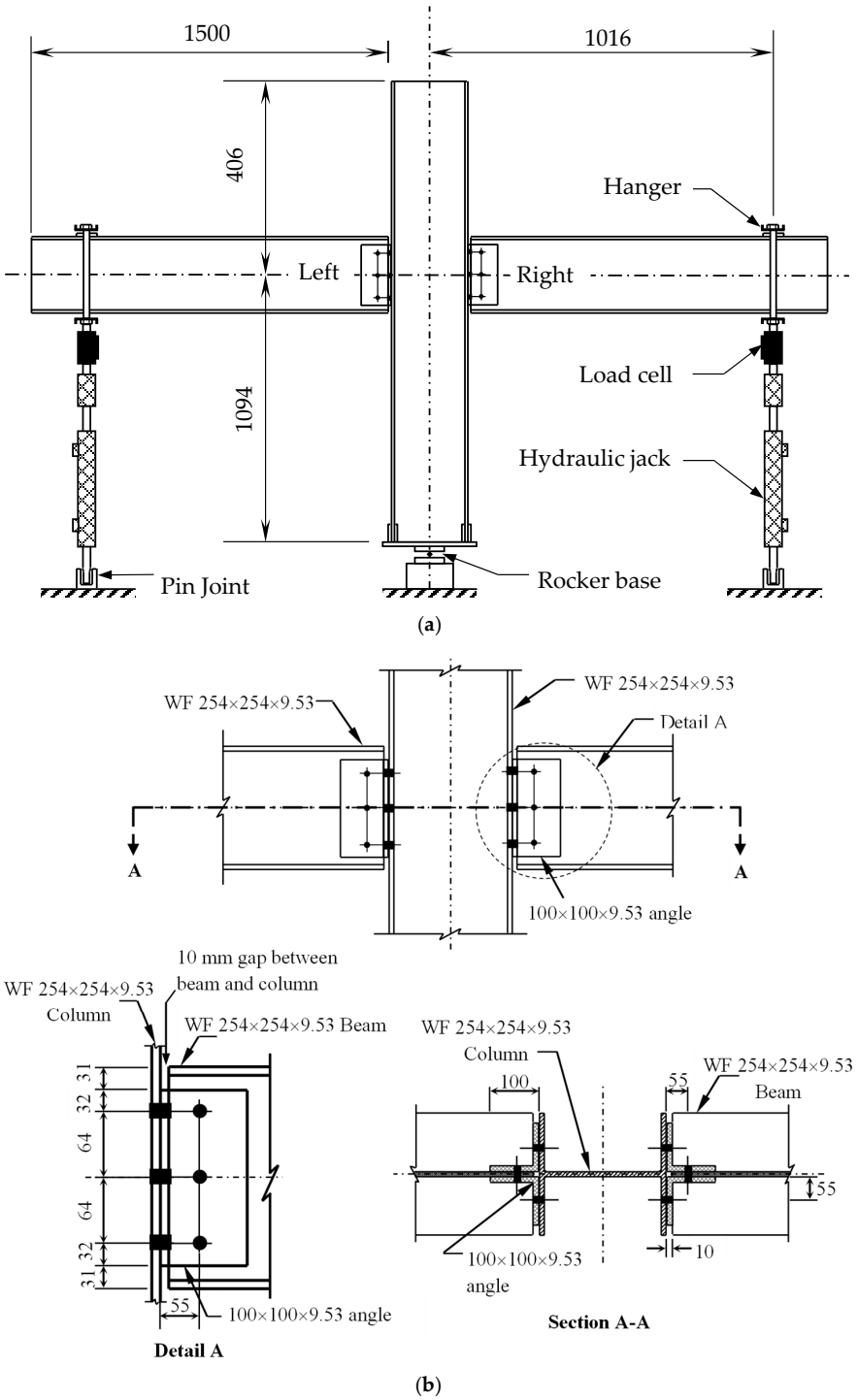


Figure 2. Schematic diagram of beam–column joint test—all dimensions are in mm [18]: (**a**) test setup using back-to-back cantilever beams and (**b**) connection detailing for beam-to-column joints.

2.2. Geometry

The beam-to-column joint geometry was modelled in ABAQUS by creating individual parts in the *Parts* module and assembling them in the *Assembly* module.

2.2.1. Beam and Column

The beam and column were modelled as three-dimensional deformable solid parts representing pultruded I-sections. Each component was defined with the required geometric dimensions and fillet radii between the web and flanges to replicate the actual cross-sectional shape. The sections were extruded to the specified length along the global Z-direction.

2.2.2. Web Cleat

Web cleats were represented as equal-leg angle sections modelled using three-dimensional deformable solids. The geometry included rounded internal corners to reflect the manufactured fillet curvature. The cleats were extruded to their required length consistent with the experimental configuration.

2.2.3. Steel Bolts

Steel bolts were modelled as solid cylindrical elements created through revolution to represent their full three-dimensional geometry. The bolts were assigned the appropriate steel material properties and positioned through the cleat and beam web holes to replicate the bolted joint assembly.

2.2.4. Steel Loading Plate

The loading plate was modelled as a rectangular solid with sufficient thickness to ensure uniform load transfer. All components were positioned and aligned to form the complete beam-to-column joint assembly for analysis.

2.3. Material Properties

The *Material* module was used to define the mechanical properties of the model, including elastic, plastic, and damage criteria.

2.3.1. FRP Beam, Column, and Cleats—Elastic Properties

The elastic properties of the composite are defined using engineering constants. For composites, isotropic elastic constants are insufficient to describe directional behaviour. Therefore, fibre-reinforced directional properties are introduced through engineering constants, lamina properties, or orthotropic material definitions to capture the anisotropic nature of the material.

Although density does not influence static analyses, it was included in the material definition to allow for dynamic or quasi-static applications if required. The elastic engineering constants for the different profiles are presented in Table 1.

Table 1. Elastic material properties for FRP profiles and cleats from Creative Composites [19].

Material Property	Input Value
Density (tonne/mm^3)	2.1×10^{-9}
Young's Modulus, E_1 (N/mm^2)	29,000
Young's Modulus, $E_2 = E_3$ (N/mm^2)	8600
Poisson's Ratio, $\nu_{12} = \nu_{13}$	0.35
Poisson's Ratio, ν_{23}	0.12
Shear Modulus, $G_{12} = G_{13}$ (N/mm^2)	3000
Shear Modulus, G_{23} (N/mm^2)	3400

In Table 1, the elastic properties of the pultruded FRP profiles are defined using orthotropic engineering constants to accurately represent the anisotropic mechanical behaviour of the material. The Young's modulus in the longitudinal direction (E_1) corresponds

to the stiffness along the primary fibre axis, which governs the load-bearing capacity of the profile. The transverse moduli (E_2 and E_3) represent the stiffness in directions perpendicular to the fibres, typically influenced by the resin and mat layers.

Poisson's ratios ν_{12} and ν_{13} describe the lateral strain in the transverse directions when the material is stretched longitudinally, while ν_{23} captures the interaction between the transverse and through-thickness directions. The shear moduli G_{12} and G_{13} quantify the resistance to shear deformation in planes involving the fibre direction, and G_{23} represents shear stiffness in the transverse–through-thickness plane. These parameters are essential for capturing the directional stiffness and deformation characteristics of pultruded FRP materials in finite element simulations.

2.3.2. FRP Beam, Column, and Cleats—Damage Properties

The Hashin failure criterion was adopted to model the progressive damage behaviour of fibre-reinforced polymer (FRP) composites under various loading conditions. This criterion distinguishes between the following four primary failure modes: fibre tension, fibre compression, matrix tension, and matrix compression. It provides a comprehensive framework for simulating the initiation and evolution of damage in pultruded GFRP materials.

Damage evolution was defined based on fracture energy values obtained from standard ASTM tests, enabling realistic representation of post-failure softening. A small stabilisation parameter was introduced to prevent numerical instabilities during simulation, with its value maintained below the minimum time increment to ensure convergence and stability.

The implementation of the Hashin model allows accurate prediction of both failure initiation and propagation in GFRP joints subjected to complex loading conditions. Although the present study focuses on monotonic loading, future research will extend the validated Hashin damage model to cyclic and seismic scenarios to assess its robustness under dynamic conditions. The adopted Hashin damage parameters for the model components are summarised in Tables 2–4.

Table 2. Hashin damage for FRP beam and column flange from Creative Composites [19].

Material Property	Input Value
Longitudinal Tensile Strength (N/mm^2)	275
Longitudinal Compressive Strength (N/mm^2)	315.7
Transverse Tensile Strength (N/mm^2)	95
Transverse Compressive Strength (N/mm^2)	122.4
Longitudinal Shear Strength (N/mm^2)	60
Transverse Shear Strength (N/mm^2)	27.5

Table 3. Hashin damage for FRP beam and column web from Creative Composites [19].

Material Property	Input Value
Longitudinal Tensile Strength (N/mm^2)	208.3
Longitudinal Compressive Strength (N/mm^2)	257.8
Transverse Tensile Strength (N/mm^2)	72.2
Transverse Compressive Strength (N/mm^2)	97.6
Longitudinal Shear Strength (N/mm^2)	48.3
Transverse Shear Strength (N/mm^2)	23.4

Table 4. Hashin damage for FRP leg angles (web cleats) from Creative Composites [19].

Material Property	Input Value
Longitudinal Tensile Strength (N/mm^2)	215
Longitudinal Compressive Strength (N/mm^2)	270
Transverse Tensile Strength (N/mm^2)	115
Transverse Compressive Strength (N/mm^2)	175
Longitudinal Shear Strength (N/mm^2) (Full section)	48.3
Longitudinal Shear Strength (N/mm^2) (through heel of angle)	23.4
Transverse Shear Strength (N/mm^2)	23.4

Tables 2–4 present the Hashin damage parameters used to model progressive failure in the pultruded FRP components of the beam–column joint. These tables list the tensile, compressive, and shear strengths in both longitudinal and transverse directions for various parts of the joint: Table 2 corresponds to the flange regions of the beam and column, Table 3 to the web regions, and Table 4 to the web cleats (equal-leg angle sections). The variation in strength values reflects the directional nature of the pultruded FRP material, which consists of continuous unidirectional fibres and mat layers. Accurate definition of these parameters is essential for capturing the onset and evolution of fibre and matrix failures under different loading conditions, as governed by Hashin's failure criterion in the finite element model.

2.3.3. Steel Bolts and Loading Plates

A bilinear elastic–perfectly plastic material model was used to define the behaviour of the steel components. The initial linear portion of the stress–strain curve was characterised by the elastic modulus up to the yield stress, beyond which the material was assumed to behave as perfectly plastic until the ultimate stress was reached. This approach effectively represents the elastic–plastic response typical of structural steel.

Both the bolts and loading plates were modelled as steel components exhibiting elastic–plastic behaviour. A density of 7.85×10^{-9} tonne/mm^3 and a modulus of elasticity of 210 GPa were assigned to all steel parts. The loading plates were modelled using S355 structural steel, while the bolts were defined as grade 8.8 high-strength steel. The detailed material properties for both components are provided in Tables 5 and 6.

Table 5. Steel Grade 355 for loading plates plastic material properties [20].

Yield Stress (N/mm^2)	Plastic Strain
355	0
470	0.2

Table 6. Steel Bolt Grade 8.8 plastic material properties [20].

Yield Stress (N/mm^2)	Plastic Strain
640	0
800	0.178

2.4. Assembling Individual Parts

The beam, column, web cleats, bolts, and loading plates were modelled as separate components and assembled to replicate the geometry of the experimental beam-to-column joint. The parts were precisely aligned to ensure accurate representation of the physical joint. Reference points were introduced at the loading locations to simulate the positions of

the hydraulic jacks used in the experimental tests. This process produced a complete three-dimensional model of the pultruded GFRP beam-to-column joint, as shown in Figure 3.

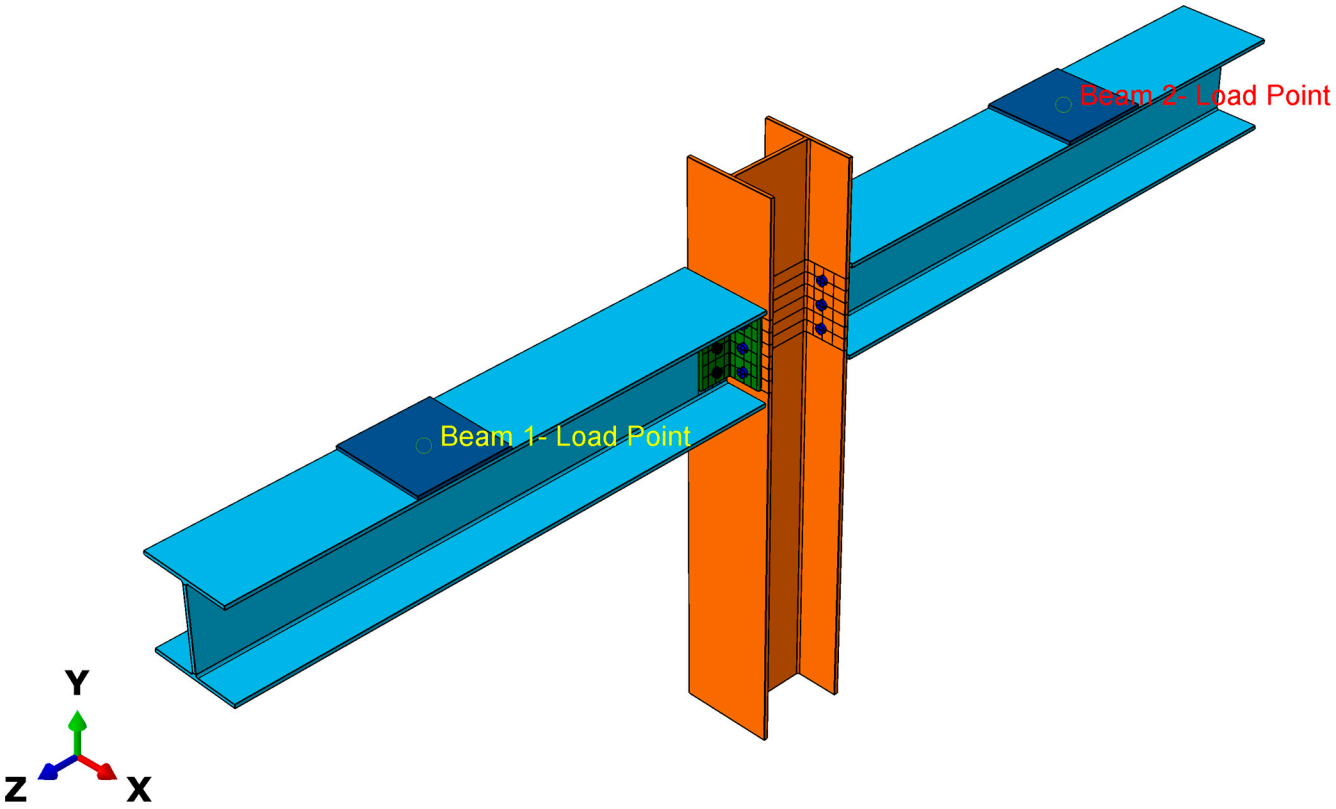


Figure 3. Beam-to-column joint after assembling all parts including loading plates.

2.5. Defining Analysis Steps

Both static and cyclic analyses were performed to evaluate the behaviour of the beam-to-column joint. The analysis procedure included the following three stages: an initial step, a bolt preload step, and a static general loading step. A bolt preload of 12.5 kN was applied to ensure proper contact between the connected surfaces, representing a finger-tight condition consistent with experimental practice. Non-linear analysis settings were used to capture material and contact nonlinearities during loading. Relevant field outputs, including stress, strain, and damage variables, were recorded for subsequent evaluation of the composite and fracture responses.

2.6. Defining Contact Interactions

Contact interactions between all connecting surfaces were modelled using a penalty frictional formulation with a hard contact pressure–overclosure relationship. A constant friction coefficient of 0.2–0.3 was used between the GFRP and steel surfaces; however, pressure-dependent friction variations observed in FRP–steel interfaces were not considered. This simplification is acknowledged as a limitation.

Tie and coupling constraints were applied to simulate the bonded and rigid connections between components. The loading plates were rigidly connected to reference points, where loads and displacements were applied to replicate the experimental conditions. This approach ensured accurate load transfer and realistic simulation of the beam-to-column joint behaviour under applied loading.

2.7. Boundary Conditions and Load Application

The model configuration included a central column with a rocker-base pinned support and two beams connected perpendicularly on either side. The rocker base allowed free rotation about the x-, y-, and z-axes, providing a realistic pinned boundary condition. Translational degrees of freedom at the column base were fully restrained to prevent movement.

Loading was applied simultaneously to both beams as downward displacements in the negative y-direction, replicating the experimental setup. Reference points were defined at the loading locations to control displacement and rotation. A vertical displacement of −50 mm was applied incrementally at each loading point to simulate the experimental loading sequence and capture the non-linear response of the joint.

2.8. Meshing and Mesh Sensitivity Analysis

The finite element (FE) models were developed and simulated using the commercial analysis software ABAQUS 6.17. The parts created included the following: (i) GFRP pultruded beam, (ii) GFRP pultruded column, (iii) GFRP web cleats, (iv) flange and web bolts (M16 grade 8.8 steel), and (v) steel loading plates. All parts were modelled with the exact sizes and dimensions used in the experimental study.

2.8.1. Meshing

Pultruded GFRP elements were meshed with eight-node continuum shell elements with reduced integration and default hourglass control (SC8R). Each ply was defined with three integration points through the thickness. The composite layups (consisting of rovings and mats) were treated as continuum shell elements, discretised into three-dimensional bodies. These elements possess only displacement degrees of freedom, but kinematic and internal energies contribute to their behaviour. As in conventional shell elements, stresses, strains, and damage variables were calculated at the integration points of each ply. Ply thickness was defined by the nodal spacing in the normal direction.

Steel parts, such as bolts and loading plates, were meshed with eight-node solid elements with reduced integration and default hourglass control (C3D8R). To reduce computational complexity, the steel components were assumed to be elastic isotropic, as the focus of the study was on the behaviour of the GFRP beam-to-column connection.

The GFRP beams were meshed with an element size of 15 × 15 mm, except at the web–flange junctions, where a finer mesh of 5 × 5 mm was applied. Each beam contained 7224 elements and 21,980 nodes. For two cantilever beams, this resulted in 14,448 elements and 43,960 nodes. Web cleats were meshed with 15 × 15 mm elements, except at the fillet radius (5 mm). Each cleat had 3004 elements and 9658 nodes; four cleats were used in total, giving 12,016 elements. Web bolts were meshed with a 2 mm size, producing 2944 elements per bolt. With six web bolts, the total was 17,664 elements. Flange bolts were meshed with the same 2 mm size, giving 2480 elements per bolt. With twelve flange bolts, this resulted in 29,760 elements. Each loading plate, meshed with 15 × 15 mm elements and 1 mm depth, contained 289 elements, giving 598 elements for both plates. In total, the complete model contained 81,712 elements. All meshed parts are shown in Figure 4.

Interfaces between the GFRP beam, the column base support, and the loading plates were defined using surface-to-surface contact with hard normal behaviour and a tangential friction coefficient of 0.2, minimising potential convergence issues due to prying action. The interface between the loading plates and the cantilever beams was defined using tie constraints, with appropriate degrees of freedom restrained. Loading was applied directly to the steel plates as displacement in the negative y-direction.

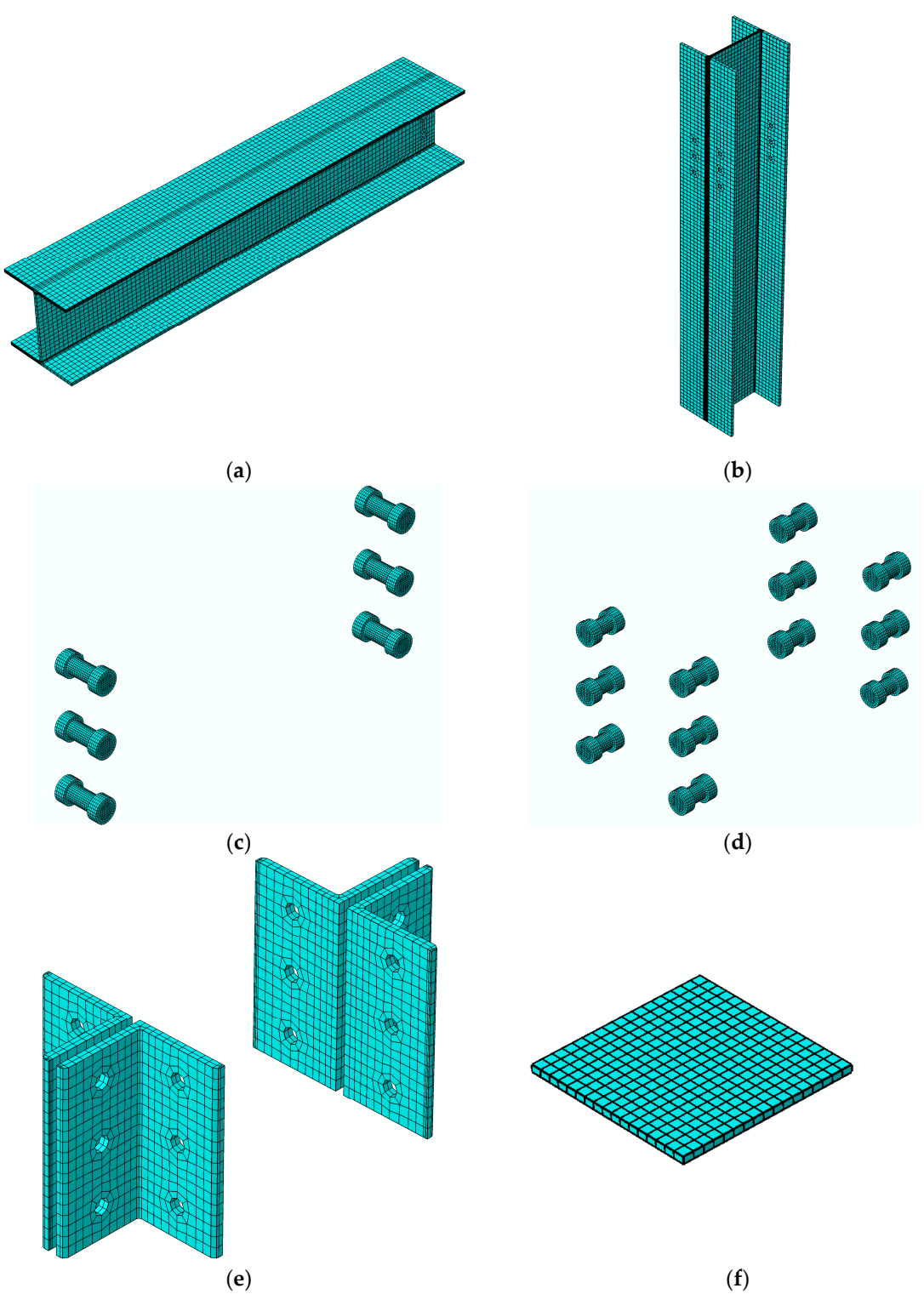


Figure 4. Meshing individual parts of beam-to-column sub-assembly: (**a**) FRP beam with bolt holes; (**b**) FRP column with bolt holes; (**c**) steel bolt for beam web; (**d**) steel bolt for column flange; (**e**) FRP web cleat (leg-angle connecting beam with column); and (**f**) steel loading plate.

2.8.2. Mesh Sensitivity Analysis

Meshing is a critical stage in ABAQUS for achieving accurate and convergent results. While straight-edged geometries are relatively simple to mesh, curved edges, fillets, and bolt geometries require additional partitioning. The partitioning technique was, therefore,

applied to subdivide the complex geometries into simpler sections, which were then meshed using the sweep method and medial axis algorithm.

Each part was meshed separately. Beams, columns, web cleats, and loading plates were meshed with global sizes of 7.5 mm and 15 mm, whereas bolts, being smaller components, were meshed with a 2 mm size. The finer 7.5 mm mesh produced results within 5% of the 15 mm mesh, but with a significantly higher computational cost. Therefore, the 15 mm mesh was adopted for the main model.

Mesh controls were assigned using hex or hex-dominated elements where possible, with structured or sweep techniques applied depending on geometry. Hourglass control was set to the enhanced/default method. Element deletion was enabled to simulate damage progression in the GFRP material using the Hashin damage criterion, capturing tensile and compressive fibre and matrix failures.

Finally, seeding was applied to activate meshing for each part and ensure consistent discretisation. The final meshed model of beam–column joint is shown in Figure 5.

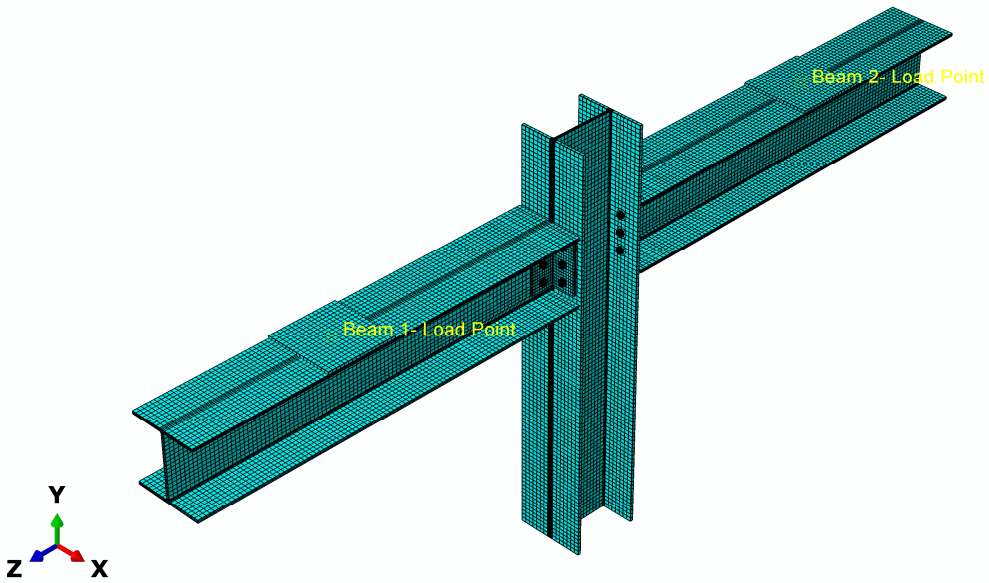


Figure 5. Final meshed finite element model for FRP beam–column sub-assembly.

2.9. Job Definition and Simulation

The finite element analyses were executed using the ABAQUS solver with double-precision settings to ensure numerical accuracy. The input files were verified prior to execution to confirm model integrity and convergence stability during the simulation process.

2.10. Visualisation and Result Extraction

Following the analysis, results were extracted from the output database to evaluate the structural response of the joint. Load–displacement and moment–rotation relationships were derived from the numerical output to compare with experimental findings.

Failure modes were examined by inspecting stress and damage distributions within the web cleats. The Hashin damage outputs provided detailed insight into the initiation and propagation of fibre and matrix failures, allowing assessment of localised damage development in the joint configuration.

2.11. Validaiton with Experiments

This section presents the numerical results of the simulation, illustrating the configuration and behaviour of the GFRP beam-to-column joint reinforced with GFRP web cleats. The analysis aims to assess both the linear and non-linear moment–rotation response, as

well as the progressive damage predicted by Hashin's failure criterion. The numerical results, including moment–rotation (M-ϕ) curves, are compared with the experimental data reported by Qureshi and Mottram [18] to validate the numerical model.

2.11.1. Moment Versus Rotation Curves

Static non-linear analysis was performed to determine the moment resistance capacity, the initial stiffness (S_i), and the ultimate moment (M_{max}). The initial stiffness was calculated using the expression $S_i = M_i/\phi_i$, where M_i and ϕ_i correspond to the moment and rotation at the linear stage of the connection. The analysis also provided the maximum rotation (ϕ_{max}) and the failure modes of the joint, including the delamination points of the sections. Bolt loads and stresses were not included, as the model focuses on the behaviour of the GFRP pultruded sections (beams, columns, and web cleats).

Figures 6 and 7 present the M-ϕ curves for the numerical and experimental results for the left- and right-side joint, respectively. For left-hand joints, the maximum moment (M_{max}) from the numerical analysis was approximately 1.78 kNm compared to 1.76 kNm in the experiment, representing a variation of around 5%. The maximum rotation (ϕ_{max}) was 42.70 mrad numerically, slightly higher than the experimental value of 41.20 mrad, a difference of approximately 2%.

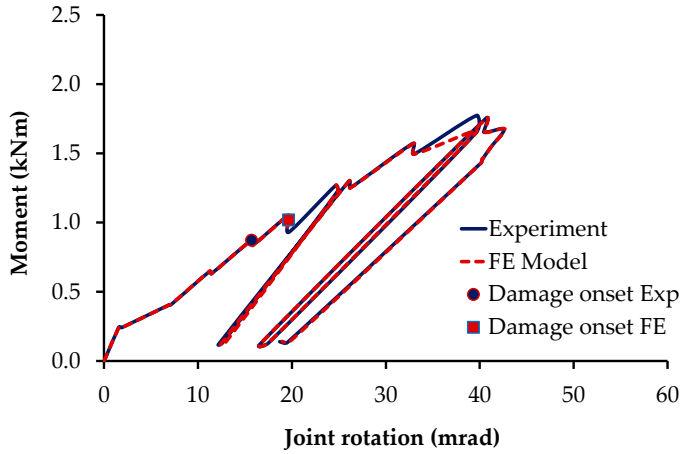


Figure 6. Experiment versus numerical moment–rotation curve for left-side joint.

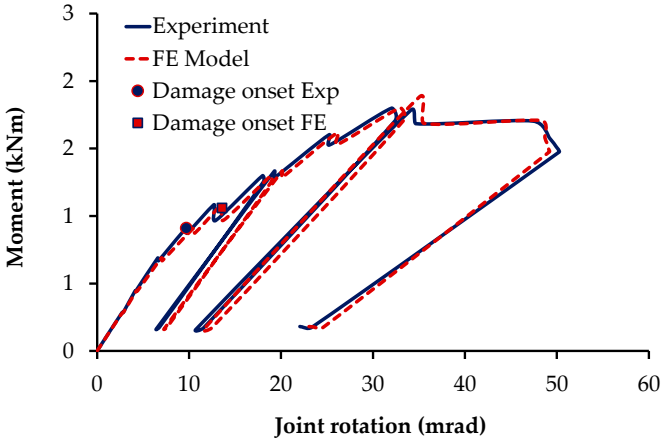


Figure 7. Experiment versus numerical moment–rotation curve for right-side joint.

The right-hand curve illustrates the maximum moment capacity as approximately 1.80 kNm for both the numerical and experimental results. When comparing the maximum rotation, the numerical value of 49.17 mrad shows a small variation from the experimental

value of 50.25 mrad. The moment–rotation behaviour on both the left and right sides from the FE analysis show close agreement with the experimental results. The damage onset is shown by a circle and square symbol in Figures 6 and 7. Both the numerical and experimental results show a 10% variation in the onset of damage in web cleats.

2.11.2. Delamination and Failure Modes

The failure modes and patterns observed in the numerical models closely matched those in the experimental setups, although the fracture values in the experiments are slightly lower than those predicted numerically. Failure was predominantly governed by shear stresses, and Hashin's failure criterion captured compression, tension, fibre, and matrix failures in the numerical simulation. In the model, damaged elements are colour-coded, as follows: red indicates fully damaged elements (D = 1.0), while blue represents undamaged elements (D = 0.0), as seen in Figures 8–11.

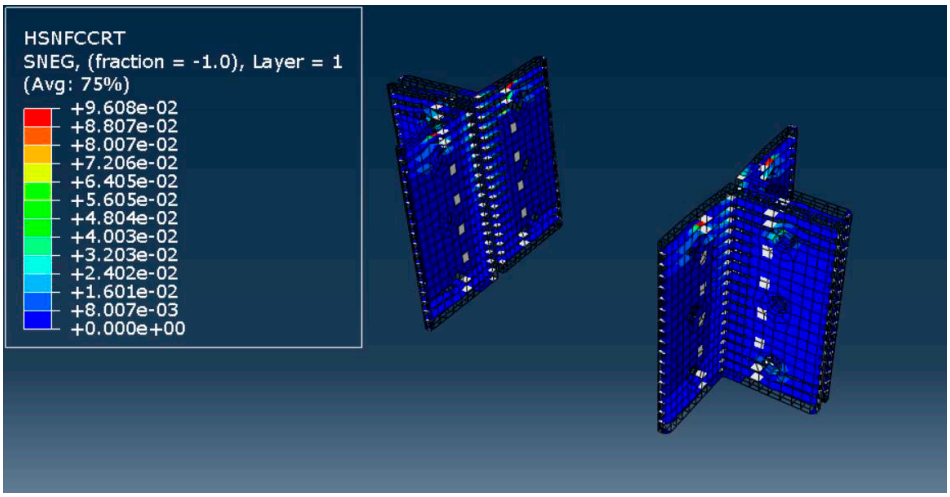


Figure 8. Hashin's compressive fibre failure at web cleat top.

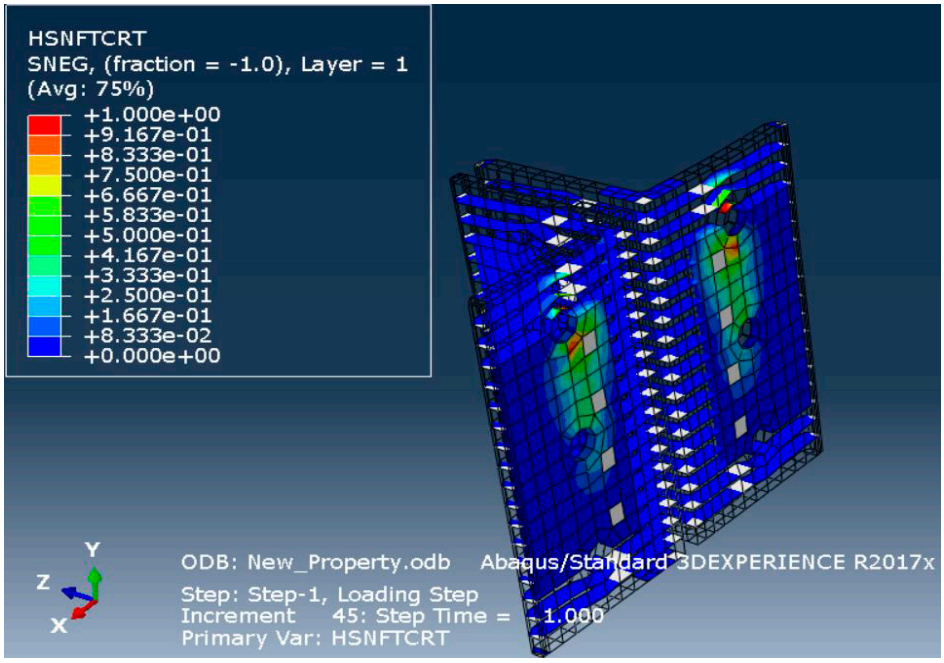


Figure 9. Hashin's tensile fibre failure in the vicinity of web cleat hole.

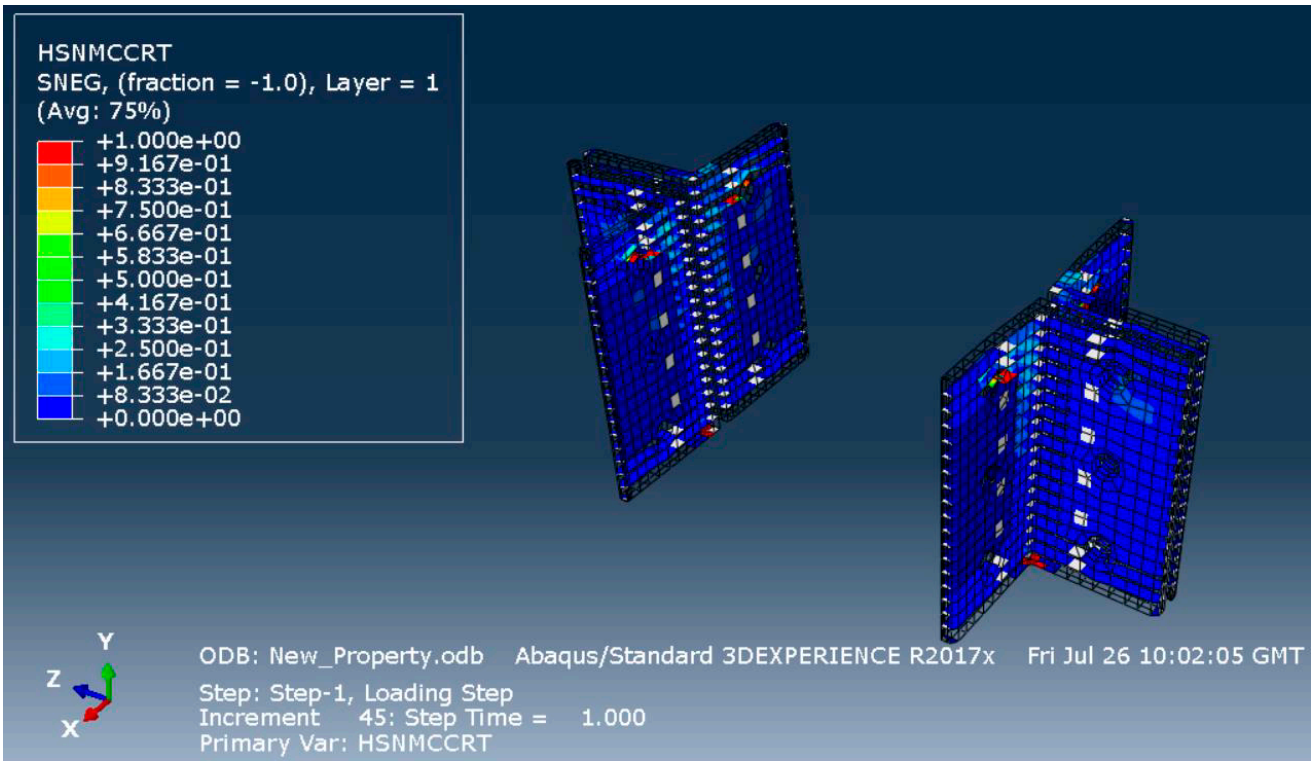


Figure 10. Hashin's compressive matrix failure at web cleat.

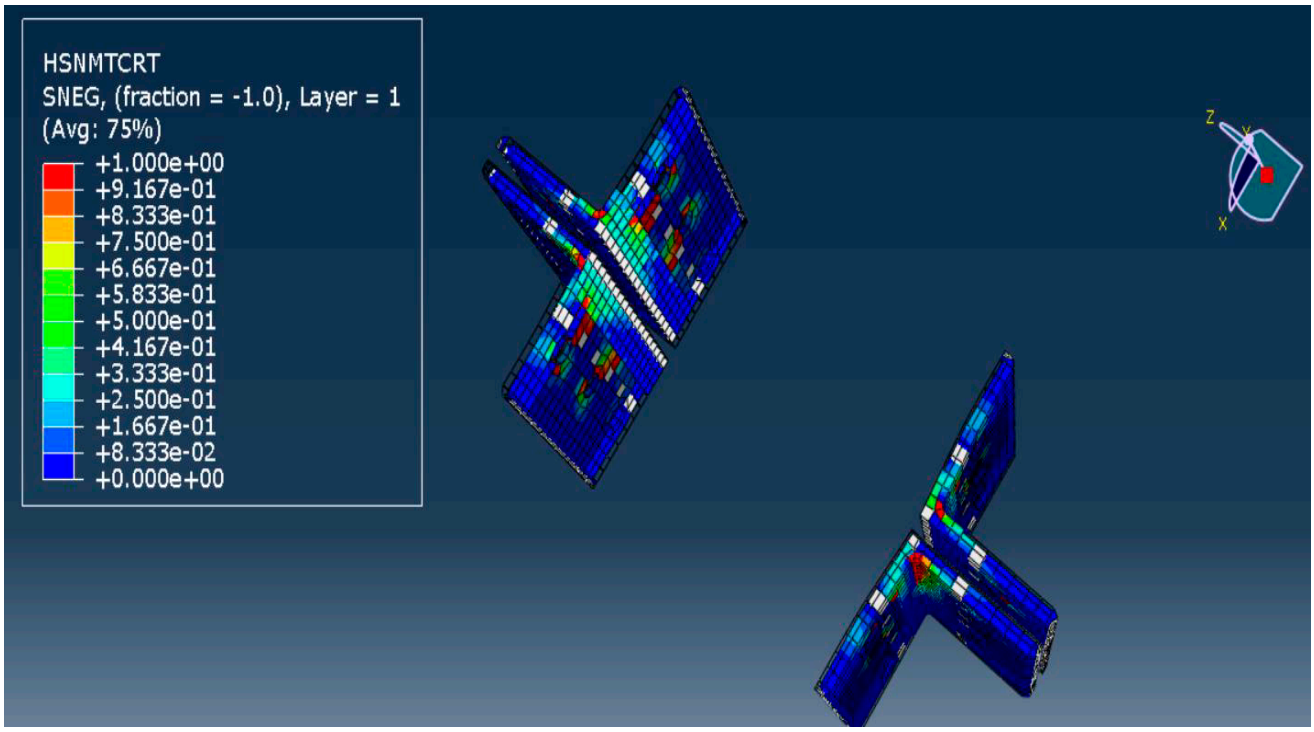


Figure 11. Hashin's tensile matrix failure at the top fillet radius of the web cleat.

In the experimental setup, a hairline crack was observed at the top fillet radius of the web cleats following the initial stiffness (S_i) in the linear region. The stiffness reduced as non-linearity developed in the moment–rotation curve. Similarly, in the numerical simulation, delamination occurred at the top fillet radius of the web cleat, although the numerical values differed slightly. According to Hashin's criterion, tension failures were

typically complete, while compression failures were partial (D = 0.5 – 0.75). Matrix and fibre failures were fully developed with D = 1.0. Compressive and tensile damage in web cleats is presented in Figures 8–11.

The predicted failure modes in the numerical model closely matched those observed experimentally, with both exhibiting delamination at the fillet radius of the web cleats and progressive fibre/matrix failures. Minor discrepancies were noted in the extent of matrix cracking, which may be attributed to local manufacturing imperfections not captured in the model. The anisotropic behaviour of pultruded FRP was explicitly accounted for by defining orthotropic elastic properties and implementing Hashin's progressive damage criterion. This approach enabled differentiation between fibre tension/compression and matrix tension/compression failures, ensuring realistic simulation of damage initiation and evolution under complex loading conditions.

Overall, the numerical and experimental results were in close agreement, with variations below 10%. The validated numerical model was, therefore, used for subsequent parametric studies to investigate moment–rotation behaviour, joint stiffness, and potential improvements to the GFRP pultruded beam-to-column joint configuration.

3. Parametric Study

A parametric study was conducted by varying the connection geometry, bolt size, and bolt–hole clearance. The aim was to examine, in detail, the behaviour of the FRP pultruded beam-to-column connection with FRP web cleats by adjusting key parameters that influence its performance. This examination sought to evaluate the effects of these parameters on stiffness, strength, ductility, and failure modes and to assess the sensitivity of the connection response to such variations.

In general, several connection techniques exist for structural joints. Welded connections are common in steel structures but are not feasible for FRP frames, as the heat generated during welding would damage the glass fibres and resin in pultruded elements. Bonded connections have been reported in the literature—for example, by Zheng [21]—as adequate for pultruded FRP sections, providing uniform stress transfer. However, their long-term durability is uncertain, which makes them less suitable for FRP applications. Consequently, bolted connections, adapted from steel structures, are widely used. In such connections, bolt–hole clearance plays a key role in accommodating stresses around the bolt holes.

Previous studies [4,22–24] identified the following three key parameters influencing the behaviour of bolted FRP joints: connection geometry, bolt size, and bolt–hole clearance. In this study, the connection geometry, fibre orientation, and bolt–hole clearance were systematically varied to evaluate their influence on the performance of the beam-to-column joint.

3.1. Connection Geometry

In this parametric study, the overall connection configuration and dimensions were modified to reflect the availability of commercially produced sections for potential future applications. The lengths and widths of the FRP beam and column sections were kept constant, while the size and thickness of the web cleat leg angle were varied. For this numerical simulation, an equal-leg angle web cleat of 150 × 150 × 12.7 mm was used, whereas the experimental beam-to-column tests in Qureshi and Mottram [18] employed a 100 × 100 × 9.53 mm web angle.

The model was designated as Wmj254_3M16_Wc150 (where WC denotes web cleat), representing a major-axis beam-to-column joint with a 254 × 254 × 9.53 mm wide-flange FRP section, connected using three M16 grade 8.8 bolts and a 150 × 150 × 12.7 mm web cleat.

The moment–rotation (*M*-ϕ) curve for the model Wmj254_3M16_WC150, shown in Figure 12, represents the joint with a 150 × 150 × 12.5 mm equal-leg angle web cleat. For this configuration, damage initiation was observed in the left beam at a rotation of approximately 8.9 mrad and a moment of about 0.78 kNm. Non-linearity began at around 0.68 kNm, with no delamination detected up to that point. The subsequent drop in moment indicates creep relaxation in the web cleats, followed by progressive damage. At the same stage, the right beam exhibited a rotation of 6.8 mrad with a corresponding moment of approximately 0.7 kNm.

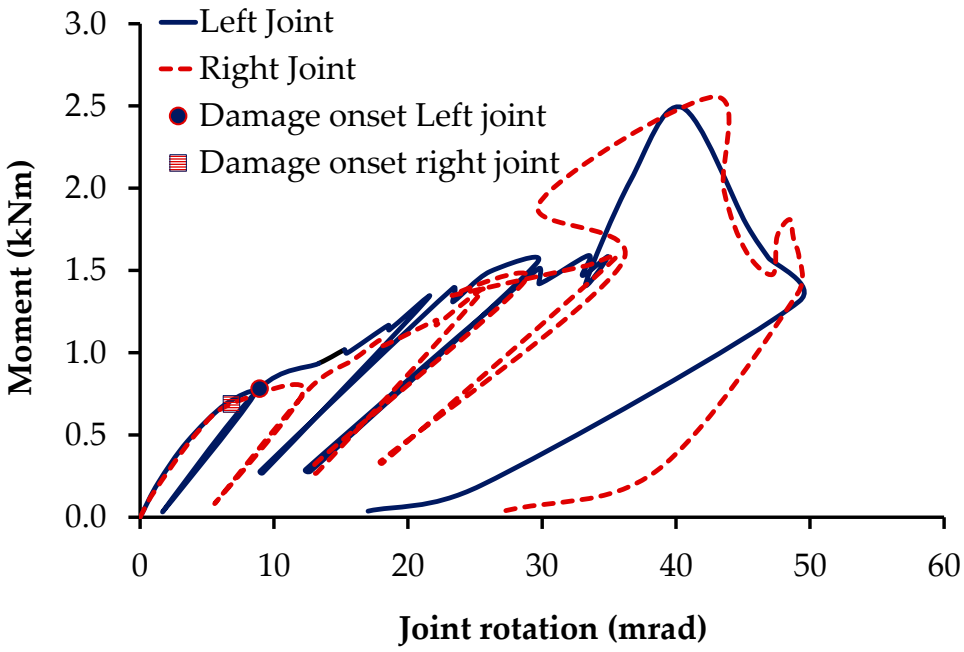


Figure 12. Moment–rotation behaviour for the model Wmj254_3M16_WC150.

The *M*-ϕ responses of both joints (left and right) remained comparable until delamination of the FRP material occurred. The failure was attributed to extensive delamination damage at the top of the web cleats, particularly around the fillet radius. The initial stiffness (S_i) for this configuration was obtained directly from the numerical curve. In ABAQUS, bolt and hole effects are automatically accounted for, eliminating the need for slip–rotation compensation, which was necessary in the experimental tests.

These results, together with the *M*-ϕ response, indicate that the failure moment in this case is slightly higher than that of the control experiment. Therefore, increasing the thickness of the web cleats enhances the initial stiffness (S_i), although the ultimate failure remains governed by delamination.

3.2. Bolt Size

In the experimental setup [18], M16 grade 8.8 bolts with 3 mm thick washers were used. For this parametric study, the bolts were replaced with M18 grade 8.8 bolts while retaining the 3 mm thick washers to study the behaviour of joints with a different bolt size. The model was designated as Wmj254_3M18_BS (Bolt Size).

The moment–rotation (*M*-ϕ) curve for the model Wmj254_3M18_BS, shown in Figure 13, illustrates the joint configuration with three M18 grade 8.8 bolts and 3 mm thick washers. The connection comprised two cantilever beams and a central column of 254 × 254 × 9.53 mm, connected using 100 × 100 × 9.53 mm equal-leg angle web cleats. The only alteration in this configuration was the increase in bolt size, which also required an increase in hole diameter with the appropriate clearance.

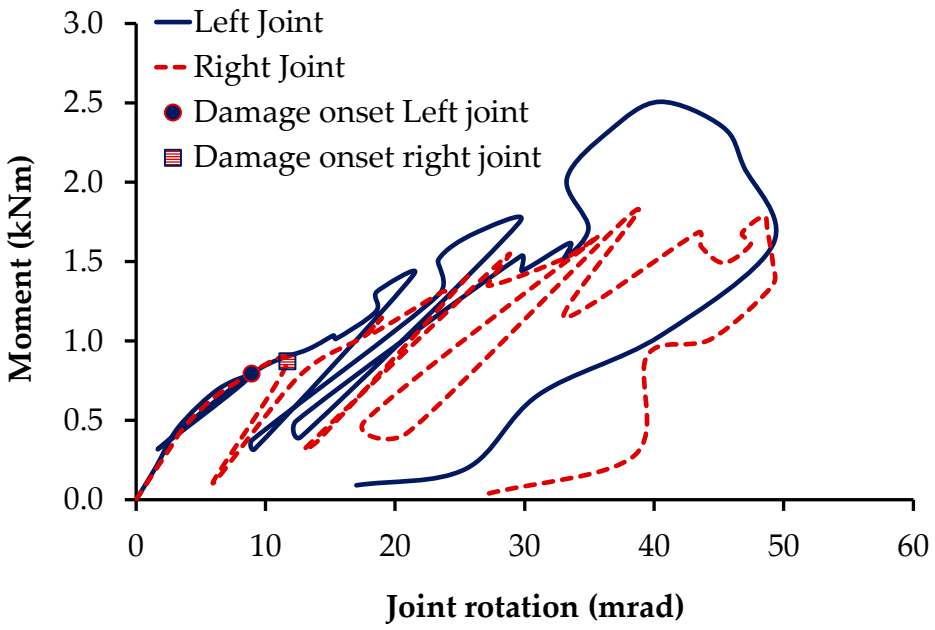


Figure 13. Moment–rotation behaviour for the model Wmj254_3M18_BS.

For this model, damage initiation in the left beam was observed at a rotation of approximately 8.9 mrad and a moment of 0.79 kNm. Non-linearity began at around 0.75 kNm, and a delamination point occurred early at a low moment. This was attributed to the larger bolt diameter, where significant pre-tension in the shank caused brittle behaviour. On the right beam, delamination onset was recorded at around 0.87 kNm and 11.7 mrad.

Slip rotation was detected in the FEM simulation but compensated automatically by the convergence solver, and the corrected response was obtained. The ultimate moment resistance reached approximately 2.5 kNm for the left side and 1.8 kNm for the right side. From the M-ϕ curve, the initial stiffness (S_i) was determined, along with the initial moment (M_i) and initial rotation (ϕ_i) prior to delamination. Failure occurred at the top of the web cleats, concentrated around the curvature of the fillet radius.

The fluctuation observed in Figure 13 represents a temporary stiffness variation caused by slip rotation and bolt pre-tension effects. Larger bolt diameters increase localised pressure at the bolt–hole interface, leading to a brief reduction in stiffness followed by recovery as the joint redistributes load. This phenomenon highlights the sensitivity of FRP joints to bolt size and clearance, particularly in the early non-linear stage prior to delamination.

When considering bolt size as the key parameter, slip rotation would typically be expected. However, no significant slip was observed in this case. This finding aligns with the observations of Qureshi and Mottram [18], who noted that slip rotation represents a critical consideration in the design of simple pultruded FRP joints, requiring careful preparation and allowance in practical applications.

3.3. Bolt–Hole Clearance

In the parental model used for experimental validation, the bolt–hole clearance was defined as 0 mm in the beam and 1 mm in the column flange to facilitate assembly of the joint components. In this parametric study, the clearance was increased by 1 mm, giving 2 mm, clearance in the column flanges while maintaining 0 mm clearance in the beam. The model was designated as Wmj254_3M16_BC2.0 (bolt–hole clearance).

The moment–rotation (M-ϕ) curve for the model Wmj254_3M16_BC2.0, shown in Figure 14, illustrates the same connection configuration used to validate the numerical model. The joint consisted of a 254 × 254 × 9.53 mm cantilever beam and column made of

GFRP pultruded sections, connected with 100 × 100 × 9.53 mm equal-leg FRP angles. In the experiment, M16 grade 8.8 steel bolts were used; in this parametric model, the alteration introduced was a bolt–hole clearance of 2 mm on both the beam web and the column flange, following observations by Zheng [21] that bolt–hole clearance significantly affects the moment–rotation response and initial stiffness.

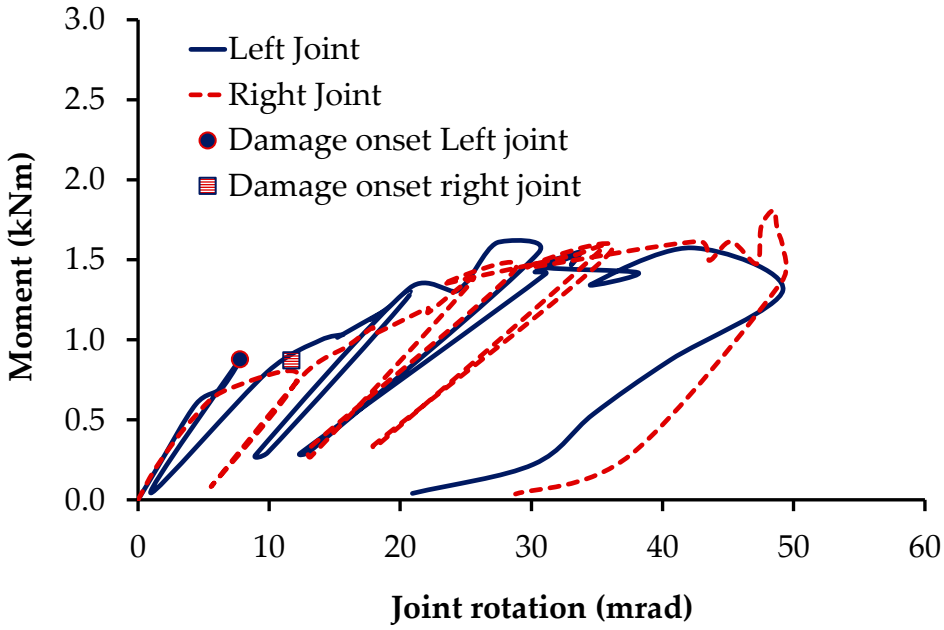


Figure 14. Moment–rotation behaviour for the model Wmj254_3M16_BC2.0.

Damage initiation in this model was observed at a moment of approximately 0.88 kNm and a rotation of 7.80 mrad on the left beam. On the right beam, the onset occurred at around 0.69 kNm and 6.9 mrad. Slip rotation due to bolt–hole clearance was present, arising from prying action, but this effect was automatically compensated by the non-linear convergence solver in ABAQUS.

The ultimate moment resistance showed no significant variation, reaching 1.60 kNm and 1.80 kNm for the left and right beam, respectively. The initial stiffness (S_i) values were obtained from the M-ϕ curves, along with the initial moment (M_i) and rotation (ϕ_i) values prior to delamination. The failure mode was consistent with other numerical models, with delamination occurring at the fillet curvature radius of the web cleats.

3.4. Joint Properties

The primary objective of each numerical model was to evaluate the joint properties, including parametric models where key factors were altered to examine their influence on the joint behaviour and the moment resistance of GFRP pultruded sections. The maximum and minimum values of the initial stiffness (S_i) were calculated using the relation ($S_i = M_i/\phi_i$), where M_i and ϕ_i are obtained from the linear region of the M–ϕ curve.

The damage onset properties, defined as the moment (M_j), rotation (ϕ_j), and stiffness (S_j) at the point where material failure was first observed, were also recorded. In addition, the maximum moment capacity (M_{max}) and the corresponding maximum rotation (ϕ_{max}) were identified for each joint configuration.

In Tables 7–9, the results of the three numerical models with different key factors influencing the joint properties of the connection are summarised from their respective simulations and moment–rotation curves. For all three models, the initial moment (M_i) was found to be approximately 0.8 kNm, with a coefficient of variation (CV) of less than

5%. The average maximum moment capacity (M_{max}) recorded at failure was 2.48 kNm, 2.04 kNm, and 1.71 kNm for the modified web cleat thickness and size, bolt size, and bolt–hole clearance models, respectively, with CV < 10%. These results indicate that the introduced parametric changes did not significantly alter the overall moment resistance of the beam-to-column connection configuration.

Table 7. Joint properties for Wmj254_3M16_WC150 beam-to-column joint configuration.

Specimen Label (1)	M_i (kN m) (2)	ϕ_i (mrad) (3)	$S_i = M_i/\phi_i$ (kN m/rad) (4)	M_j (kN m) (5)	ϕ_j (mrad) (6)	$S_j = M_j/\phi_j$ (kN m/rad) (7)	M_{max} (kN m) (8)	ϕ_{max} (mrad) (9)
Wmj254_3M16_WC150 (Left)	0.75	7	107	0.93	13.3	70	2.45	40.4
Wmj254_3M16_WC150 (Right)	0.71	6.9	103	0.96	15.8	61	2.51	42.8
Mean of 2	0.73	6.95	105	0.95	14.5	66	2.48	41.6
CV	3.8%	1%	2.7%	2.4%	12%	9.7%	1.7%	4%

Table 8. Joint properties for Wmj254_3M18_BS Beam-to-column joint configuration.

Specimen Label (1)	M_i (kN m) (2)	ϕ_i (mrad) (3)	$S_i = M_i/\phi_i$ (kN m/rad) (4)	M_j (kN m) (5)	ϕ_j (mrad) (6)	$S_j = M_j/\phi_j$ (kN m/rad) (7)	M_{max} (kN m) (8)	ϕ_{max} (mrad) (9)
Wmj254_3M18_BS (Left)	0.75	7.2	104	0.95	13.4	71	2.03	40.4
Wmj254_3M18_BS (Right)	0.7	7	100	0.87	11.70	74	2.04	48.7
Mean of 2	0.725	7.1	102	0.91	12.5	72.5	2.035	44.5
CV	4.9%	2%	2.8%	6.2%	9.6%	6.9%	0.3%	13.1%

Table 9. Joint properties for Wmj254_3M16_BC Beam-to-column joint configuration.

Specimen Label (1)	M_i (kN m) (2)	ϕ_i (mrad) (3)	$S_i = M_i/\phi_i$ (kN m/rad) (4)	M_j (kN m) (5)	ϕ_j (mrad) (6)	$S_j = M_j/\phi_j$ (kN m/rad) (7)	M_{max} (kN m) (8)	ϕ_{max} (mrad) (9)
Wmj254_3M16_BHC (Left)	0.8	7.2	111	0.94	13.81	68	1.61	27.3
Wmj254_3M18_BHC (Right)	0.76	8.1	94	0.96	15.87	60.5	1.81	48.
Mean of 2	0.78	7.65	102.5	0.95	14.84	64.25	1.71	37.85
CV	3.6%	8.3%	12%	1.5%	9.7%	8%	8%	39%

The major variation identified from the full-scale model simulations was in the maximum rotation (ϕ_{max}), which ranged from 27 to 49 mrad. The maximum displacement was limited to 50 mm in order to obtain a clearer understanding of the connection behaviour. The CV of the initial stiffness (S_i) was less than 3% for the Wmj254_3M16_WC150 and Wmj254_3M18_BS models. However, for the Wmj254_3M16_BC model, the CV was about 12%, a variation that occurred only within the linear region of the moment–rotation curve, without delamination in the web cleats. To enhance joint performance beyond the non-linear stage, the mean and CV of the stiffness at damage onset (S_j) were observed to vary by less than 10% across all three models, demonstrating comparable behaviour.

The key finding of this parametric numerical analysis is that stiffness is more sensitive to changes in connection parameters than moment resistance. One of the main objectives of this study is, therefore, to develop an optimised connection design with respect to the joint properties of pultruded FRP beam-to-column connections using web cleats. Furthermore, increasing joint stiffness can be achieved by adjusting the web cleat geometry—such as increasing thickness and leg length—or by employing larger-diameter bolts. These adjustments enhance the load-carrying capacity and the initial stiffness of the joint, while appropriate design optimisation ensures material costs and overall structural weight remain reasonably low.

3.5. Joint Classification

The rotational stiffness (S_i) values obtained from the tables classify the joints as nominally pinned connections. According to Eurocode 3, Part 1–8 [25], the initial rotational stiffness at service load, $S_{i,ini}$, is calculated using the expression $S_i = M_i/\phi_i$. Based on the design specification for steel connections, if $S_{i,ini}$, $L/EI \leq 0.5$, where EI/L is the flexural stiffness of the beam member, the joint is considered nominally pinned.

For a beam with a span-to-depth ratio of 20, the span (L) is 5.90 m for a 254 mm deep wide flange (WF) section. From the property table, the flexural modulus of elasticity (E) of the WF section is 29 kN/mm^2 and the second moment of area (I) is approximately 8.34×10^7 mm^4. This gives a nominal pinned stiffness of about 230 kNm/rad.

When the span is increased to 10 m, the stiffness limit reduces to about 120 kNm/rad for the 254 × 254 × 9.53 mm WF section. In comparison, the three numerical models produced initial stiffness (S_i) values in the range of 94–111 kNm/rad. These values fall within the defined limits, confirming that the joint detailing is classified as nominally pinned.

4. Conclusions

This study advances previous research by successfully modelling full-scale pultruded FRP beam-to-column joints using progressive damage analysis. Earlier works, such as Mendes et al. [26], highlighted difficulties in simulating joint stiffness and failure due to material discontinuities and uncertain fracture energy definitions. Eskenati et al. [11] investigated bonded and bolted joints but did not apply damage evolution models. In contrast, our validated finite element model integrates Hashin's criterion with fracture energy-based damage evolution, accurately predicting delamination and failure modes. The parametric study reveals that joint stiffness is sensitive to cleat geometry and bolt characteristics, offering practical guidance for optimising FRP connection design.

The following conclusions are drawn from this research:

1. The proposed FEM accurately reproduces experimental moment–rotation curves, stiffness, and failure modes, with discrepancies below 10%, confirming its reliability for structural design applications.
2. Delamination at the fillet radius of FRP cleats is the dominant failure mechanism, effectively captured by Hashin's progressive damage model.
3. Quantitative analysis shows that variations in cleat size, bolt size, and bolt–hole clearance have minimal impact on ultimate moment capacity (CV < 10%) but significantly influence initial stiffness (up to 15% variation), highlighting the importance of connection detailing for serviceability.
4. Increasing cleat thickness and bolt diameter improves stiffness, while bolt–hole clearance introduces slip effects without compromising strength.
5. All joints classify as nominally pinned per Eurocode 3, with rotational stiffness values ranging from 94 to 111 kNm/rad.
6. The validated FEM framework offers a cost-effective alternative to extensive experimental testing and provides actionable insights for optimising FRP joint design, advancing the development of reliable design guidelines for pultruded FRP structures.

Author Contributions: Conceptualisation, writing—original draft preparation, writing—review and editing, supervision and project administration, J.Q.; methodology, software, validation, formal analysis, investigation and data curation, K.M.M. All authors have read and agreed to the published version of the manuscript.

Funding: This research received no external funding.

Data Availability Statement: The experimental data is available at https://doi.org/10.1016/j.conbuildmat.2014.12.057.

Acknowledgments: The authors would like to thank the University of East London for providing the facilities that made this research possible.

Conflicts of Interest: The authors declare no conflicts of interest.

References

1. Bank, L.C. *Composites for Construction—Structural Design with FRP Materials*; John Wiley & Sons: Hoboken, NJ, USA, 2006.
2. Mottram, J.T. Does Performance-Based Design with FRP Components and Structures Provide Any New Benefits and Challenges? *Struct. Eng.* **2011**, *89*, 23–27. [CrossRef]
3. Mosallam, A. *Design Guide for FRP Composite Connections*; American Society of Civil Engineers: Reston, VA, USA, 2011; ISBN 978-0-7844-0612-0.
4. Turvey, G.J.; Cooper, C. Review of Tests on Bolted Joints between Pultruded GRP Profiles. *Proc. Inst. Civ. Eng. Struct. Build.* **2004**, *157*, 211–233. [CrossRef]
5. Mottram, J.T.; Zheng, Y. State-of-the-Art Review on the Design of Beam-to-Column Connections for Pultruded Frames. *Compos. Struct.* **1996**, *35*, 387–401. [CrossRef]
6. Turvey, G.J. Analysis of Pultruded Glass Reinforced Plastic Beams with Semi-Rigid End Connections. *Compos. Struct.* **1997**, *38*, 3–16. [CrossRef]
7. Bank, L.C.; Mosallam, A.S.; Gonsior, H.E. Beam-to-Column Connections for Pultruded FRP Structures. In Proceedings of the Proc. 1st Materials Engineering Congress, ASCE, Denver, CO, USA, 13–15 August 1990; pp. 804–813.
8. Mottram, J.T.; Zheng, Y. Further Tests on Beam-to-Column Connections for Pultruded Frames: Web-Cleated. *J. Compos. Constr.* **1999**, *3*, 3–11. [CrossRef]
9. Qureshi, J.; Nadir, Y.; John, S.K. Cyclic Response of Bolted and Hybrid Pultruded FRP Beam-Column Joints between I-Shaped Sections. *Fibers* **2021**, *9*, 66. [CrossRef]
10. Qureshi, J. A Review of Fibre Reinforced Polymer Structures. *Fibers* **2022**, *10*, 27. [CrossRef]
11. Eskenati, A.R.; Mahboob, A.; Bernat-Maso, E.; Gil, L. Experimental and Numerical Study of Adhesively and Bolted Connections of Pultruded GFRP I-Shape Profiles. *Polymers* **2022**, *14*, 894. [CrossRef] [PubMed]
12. Matharu, N.S.; Mottram, J.T. Plain and Threaded Bearing Strengths for the Design of Bolted Connections with Pultruded FRP Material. *Eng. Struct.* **2017**, *152*, 878–887. [CrossRef]
13. Coelho, A.M.G.; Mottram, J.T. Numerical Evaluation of Pin-Bearing Strength for the Design of Bolted Connections of Pultruded FRP Material. *J. Compos. Constr.* **2017**, *21*, 04017027. [CrossRef]
14. Duan, J.; Yang, D.; Liu, X.; Xiang, P. Seismic Energy Dissipation and Hysteresis Performances of Distinctly Shaped Steel-Reinforced Concrete Column–Beam Joints under Cyclic Loading. *Buildings* **2024**, *14*, 2777. [CrossRef]
15. Qureshi, J.; Nadir, Y.; John, S.K. Bolted and Bonded FRP Beam-Column Joints with Semi-Rigid End Conditions. *Compos. Struct.* **2020**, *247*, 112500. [CrossRef]
16. Tang, J.; Feng, P.; Wang, Q. Beam-Column Joints of FRP Pultruded Profiles: State-of-the-Art Review, Performance Evaluation, and Design Method. *Compos. Struct.* **2025**, *370*, 119250. [CrossRef]
17. Ascione, F.; D'Aniello, M.; Feo, L.; Granata, L.; Landolfo, R. A Novel Ductile Connection for FRP Pultruded Beam-to-Column Assemblies. *Compos. Struct.* **2024**, *337*, 118091. [CrossRef]
18. Qureshi, J.; Mottram, J.T. Moment-Rotation Response of Nominally Pinned Beam-to-Column Joints for Frames of Pultruded Fibre Reinforced Polymer. *Constr. Build. Mater.* **2015**, *77*, 396–403. [CrossRef]
19. Creative Composites. *The New and Improved PulTex Pultrusion Design Manual*; Creative Pultrusions Inc.: Alum Bank, PA, USA, 2024.
20. Bishay-Girges, N.W. Improved Steel Beam-Column Connections in Industrial Structures. *Eng. Technol. Appl. Sci. Res.* **2020**, *10*, 5126–5131. [CrossRef]
21. Zheng, Y. Connection Behaviour and Frame Analysis for Structures of Pultruded Profile. Ph.D. Thesis, University of Warwick, Coventry, UK, 1998.
22. Abd-El-Naby, S.F.M.; Hollaway, L. The Experimental Behaviour of Bolted Joints in Pultruded Glass/Polyester Material. Part 2: Two-Bolt Joints. *Composites* **1993**, *24*, 539–546. [CrossRef]
23. Abd-El-Naby, S.F.M.; Hollaway, L. The Experimental Behaviour of Bolted Joints in Pultruded Glass/ Polyester Material. Part 1: Single-Bolt Joints. *Composites* **1993**, *24*, 531–538. [CrossRef]
24. Hollaway, L.C.; Head, P.R. *Advanced Polymer Composites and Polymers in the Civil Infrastructure*, 1st ed.; Elsevier Science: Oxford, UK, 2001; ISBN 978-0-08-043661-6.

25. *BS EN 1993-1-8:2005*; Eurocode 3: Design of Steel Structures—Part 1–8: Design of Joints. British Standards Institution: London, UK, 2005.
26. Mendes, J.D.R.S. Mechanical Behaviour of FRP Beam-to-Column Bolted Connections. Master's Thesis, Universidade de Lisboa, Lisbon, Portugal, 2023.

Disclaimer/Publisher's Note: The statements, opinions and data contained in all publications are solely those of the individual author(s) and contributor(s) and not of MDPI and/or the editor(s). MDPI and/or the editor(s) disclaim responsibility for any injury to people or property resulting from any ideas, methods, instructions or products referred to in the content.